Layered Manganese Oxide Intergrowth Electrodes for Rechargeable Lithium Batteries. 2. Substitution with Al

Sébastien Patoux, Mickaël Dollé, and Marca M. Doeff*

Materials Sciences Division, Lawrence Berkeley National Laboratory, University of California, Berkeley, California 94720

Received September 9, 2004. Revised Manuscript Received November 19, 2004

The structural and electrochemical characterization of layered $Li_xAl_yMn_{1-y}O_2$ compounds prepared from sodium-containing precursors is described. A quaternary phase diagram showing composition ranges for pure P2 and P3 structures and P2/P3 intergrowths obtained in the Na−Al−Mn−O system is presented. Upon ion-exchange, these compounds change to O2, O3, or O2/O3 stacking arrangements, respectively. The oxygen array in O3 and spinel structures is similar, and most of the O3 structures convert to spinel rapidly upon electrochemical cycling in lithium cells. This process is delayed somewhat by increased Al substitution, but not completely inhibited. More effective suppression of the phase transformation is observed in O2/O3 intergrowth electrodes. Additionally, the capacity retention upon cycling of cells containing intergrowth electrodes is superior to those with pure O2 structures.

I. Introduction

Layered Li_xMnO_2 has potential advantages as a positive electrode material in lithium cells (toxicity, cost, and safety) when compared with $Li_xCo_yNi_{1-y}O_2$ ($0 \leq y \leq 1$), but has only been prepared relatively recently by indirect synthesis.[1,2] The sodium counterpart, Na_xMnO_2, must first be prepared before proceeding to an ion-exchange reaction at relatively low temperatures to preserve the layered structure.[3] Depending on the value of *x*, the nature and amount of the substituent, and the conditions of preparation, nonstoichiometric layered $Na_xM_yMn_{1-y}O_2$ (M = Li, Co, Ni, Al, etc.) compounds can either adopt a P2 (space group $P6_3/mmc$) or a P3 ($R3m$) crystal structure type, where "P" refers to the trigonal prismatic environment of sodium, and "2" and "3" designate the number of transition metal sheets in a unit-cell, in agreement with the notation used for layered AMX_2 phases.[4] The corresponding lithiated phases adopt an O2 ($P6_3mc$) or O3 ($R\bar{3}m$) crystal structure type (i.e., Li is in an octahedral environment). Additionally, a layered $LiMnO_2$ compound may be prepared from α-$NaMnO_2$; these compounds have a monoclinic distortion of the normal rhombohedral (O3) symmetry, caused by the Jahn−Teller effect of the Mn^{3+} ions, and these layered oxides are designated as O′3-type ($C2/m$). Both unsubstituted layered oxides transform into the more stable orthorhombic $LiMnO_2$ and β-$NaMnO_2$ form ($Pmmn$) with corrugated structures at high temperatures.

In the first part of our study (see the companion paper[5]), we showed that intergrowth structures with different O2/O3 ratios could be prepared in the Ni- and Co-substituted manganese oxide system by adjusting the nominal quantity of sodium and/or substituent. We also highlighted the role played by the vacancies in the formation of P2 and P3 phases. As noted by Ceder et al.,[6] the O3 structure is unstable with respect to conversion into spinel upon electrochemical cycling due to their structural similarities. Both have a close-packed oxygen array with an ABCABC stacking sequence, which differ only in the distribution of the cations. The tendency of Mn^{3+} to disproportionate and the mobility of the resulting Mn^{2+} ions favor the conversion. Because O2 structures have a different oxygen array, spinel conversion does not occur, but the electrochemical capacities and rate capabilities are frequently inferior to those of O3 compounds. For example, O3-$Li_xNi_{0.2}Mn_{0.8}O_2$ delivers a discharge capacity of more than 200 mAh/g, whereas O2/O3-$Li_xNi_{0.2}Mn_{0.8}O_2$ (84/16) gives only about 135 mAh/g under the same cycling conditions. Although some of the Ni- and Co-substituted layered manganese intergrowths we investigated might represent an acceptable compromise between the phase stability of the O2 structure and the better electrochemical properties of O3, materials containing these elements are problematic for electric or hybrid vehicle applications because of high cost (Co) and poor abuse tolerance (Ni). However, intergrowths can also form when Al is used as a substituent. Al is attractive not only for reasons of cost and low toxicity but also because of the potential for improved abuse tolerance. Because Al is not electroactive, complete removal of lithium is unlikely to occur, preventing irreversible and potentially dangerous side-reactions associated with high states-of-charge, such as electrolyte oxidation or loss of oxygen from the positive electrode. Very high levels of substitution, however, are likely to result in reduced capacity for the same reasons. Thus, design of a stable, high-capacity Al-substituted manganese oxide electrode requires careful

* To whom correspondence should be addressed. E-mail: mmdoeff@lbl.gov.

(1) Armstrong, A. R.; Bruce, P. G. *Nature* **1996**, *381*, 499.
(2) Capitaine, F.; Gravereau, P.; Delmas, C. *Solid State Ionics* **1996**, *89*, 197.
(3) Eriksson, T. A.; Joo Lee, Y.; Hollingsworth, J.; Reimer, J. A.; Cairns, E. J.; Zhang, X.; Doeff, M. M. *Chem. Mater.* **2003**, *15*, 4456.
(4) Delmas, C.; Fouassier, C.; Hagenmuller, P. *Physica B* **1980**, *99*, 81.
(5) Dolle, M.; Patoux, S.; Doeff, M. M. *Chem. Mater.* **2005**, *17*, 1036.
(6) Reed, J.; Ceder, G.; Van Der Ven, A. *Electrochem. Solid-State Lett.* **2001**, *4*, 78.

10.1021/cm0484394 CCC: $30.25
Published on Web 02/08/2005

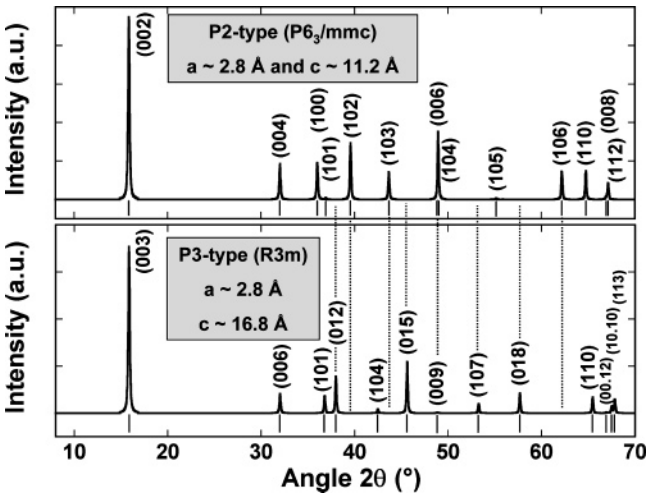

Figure 1. Calculated XRD patterns of P2-$Na_{0.7}MnO_2$ with Na(1) occupying the *2b*, Na(2) occupying the *2d*, Mn occupying the *2a*, and O occupying the *4f* sites of space group $P6_3/mmc$, and P3-$Na_{0.7}Al_{0.1}Mn_{0.9}O_2$ with all Na, Mn, Al, O(1), and O(2) atoms located in *3a* sites of space group $R3m$.

balancing not only of the O2/O3 ratio but also of the amount of substitution. In this paper, which constitutes the second part of our study, we describe the effect of substitution with aluminum on the structure of $Na_xAl_yMn_{1-y}O_2$ and $Li_xAl_yMn_{1-y}O_2$, compounds and on electrochemical performance.

II. Experimental Section

Numerous compositions with the general formula $Na_xAl_yMn_{1-y}O_2$ were synthesized by glycine−nitrate combustion.[7,8] For $x = 0.6$ and $0 \le y \le 0.60$, $x = 0.7$ and $0 \le y \le 0.30$, and $x = 0.8$ and $0 \le y \le 0.10$, y was varied by 0.02. An additional composition of $Na_{0.75}Al_{0.15}Mn_{0.85}O_2$ was also synthesized. An aqueous solution of $NaNO_3$, $Al(NO_3)_2 \cdot 9H_2O$, and $Mn(NO_3)_2$ in HNO_3, in proportion to give the expected compositions was mixed with glycine in the molar ratio 1:2 (glycine/nitrate). The solution was combusted within a stainless steel container disposed on a hot plate, by evaporating small aliquots of solution to dryness. The temperature of the combustion reaction, determined by the glycine/nitrate ratio, reached ~1300−1400 °C. The as-prepared dark-brown powder was then calcined at 800 °C for 4 h to remove any organic residue and to ensure good homogeneity.

After the synthesis of the sodium compounds, $Li_xAl_yMn_{1-y}O_2$ counterparts were prepared by ion exchange, using a 9-fold excess LiBr in ethanol under reflux (80−90 °C) for 2 days. The products were washed well with ethanol and dried at 120 °C. Exchange of $Na_{0.7}MnO_2$ and $Na_{0.7}Al_{0.02}Mn_{0.98}O_2$ was not complete under these conditions and the process was repeated under the same conditions for the former, and at 150 °C in hexanol for the latter.

X-ray diffraction (XRD) patterns at 298 K were obtained on a Philips X′Pert diffractometer ($\theta-\theta$ geometry, back monochromator) using Cu Kα radiation. Lattice parameters were determined by full pattern matching using the WinPLOTR/Fullprof suite.[9] Rietveld refinements were then performed on the intergrowth compounds to determine the approximate P2/P3 ratio. The calculated patterns shown in Figure 1 were produced using the WinPLOTR/Fullprof suite.

Inductively coupled plasma (ICP) analyses were carried out on selected samples by Desert Analytics Laboratory (Tucson, AZ) to determine exact compositions (Table 1). For the sake of convenience, we will only refer to the *nominal* rather than actual compositions throughout the discussion, unless otherwise stated. To obtain information concerning the oxidation state of manganese, density measurements were performed on the sample called $Na_{0.7}MnO_2$ (P2-type), using a 25- mL pycnometer and *N*-methyl-pyrrolidinone as solvent. The oxidation state of manganese was also determined by redox titration for P3-$Na_{0.6}Al_{0.16}Mn_{0.84}O_2$, O3-$Li_{0.6}Al_{0.16}Mn_{0.84}O_2$, P2/P3-$Na_{0.7}Al_{0.16}Mn_{0.84}O_2$, and O2/O3-$Li_{0.7}Al_{0.16}Mn_{0.84}O_2$ similar to the procedure used for $LiMn_2O_4$,[10] which was derived from the original analysis.[11] A 0.1-g portion of sample was initially dissolved in an excess of aqueous solution of $Fe^{II}SO_4(NH_4)_2(SO_4)\cdot H_2O$ (0.03 mol/L), in the presence of H_2SO_4 and H_3PO_4. All the Mn^{n+} ions were thus reduced into Mn^{2+} by the ferrous ions. The excess Fe^{2+} ions were subsequently titrated by an acidic solution (H_2SO_4) of $K_2Cr_2O_7$ (0.005 mol/L), using diphenylamine sulfonate indicator (1% in acidic solution).

Composite positive electrodes were prepared by thoroughly mixing the active material (84%) with carbon black (4%), SFG-6 graphite (4%), and polyvinylidene fluoride-Kynar 741 (8%) in *N*-methyl-pyrrolidone and extruding onto aluminum foils. Electrodes (1.8 cm^2 disks), with loadings of ~8−12 mg of active material/cm^2, were dried for 24 h at room temperature and then for 24 h at 100−120 °C under vacuum. 2032 coin cells were assembled in a helium-filled drybox (<1 ppm O_2/H_2O) using foils of Li metal as counter electrodes and Celgard 3401, saturated with 1 M $LiPF_6$ (electrolyte) in ethylene carbonate/dimethyl carbonate (1:2 in weight), as separators. To ensure reproducibility, at least three coin cells containing each sample were assembled and tested between 2.0 and 4.5 V at 21−22 °C. Lithium insertion/extraction was monitored with an Arbin BT/HSP-2043 automatic cycling data recording system operating in galvanostatic mode.

III. Results and Discussion

Structural Characterization of $Na_xAl_yMn_{1-y}O_2$. Phase-pure compounds adopt either a P2 or a P3-type structure, or are intergrowths. To distinguish these structure types quickly, the X-ray diffraction patterns of pure P2 and P3 phases were simulated (Figure 1). The most intense peaks for each phase, $(002)_{P2}$ and $(003)_{P3}$ coincide, as do several others. The $(102)_{P2}$ and $(006)_{P2}$ reflections and $(105)_{P3}$ peaks appear at different positions and are distinctive markers for each phase. XRD patterns for the nominal compositions $Na_xAl_yMn_{1-y}O_2$ ($x = 0.6$ and $0 \le y \le 0.60$, $x = 0.7$ and $0 \le y \le 0.30$, and $x = 0.8$ and $0 \le y \le 0.10$) are presented in Figure 2, and lattice parameters and phase compositions are listed in Table 1 for the pure compounds.

For $Na_{0.8}Al_yMn_{1-y}O_2$ compounds, which have high P2/P3 ratios, a hydrated phase is observed in most of the patterns. A tendency to take up water in the interlayers is characteristic of P2 phases.[12] However, this hydrated phase can simply be removed by drying at 120 °C, without any degradation. When $y \ge 0.08$, peaks attributable to impurities (possibly a phase mixture of $NaAlO_2$ and $NaMnO_2$) were found, indicating rather low limits for Al content in solid

(7) Chick, L. A.; Pederson, L. R.; Maupin, G. D.; Bates, J. L.; Thomas, L. E.; Exarhos, G. J. *Mater. Lett.* **1990**, *10*, 6.
(8) Pederson, L. R.; Chick, L. A.; Exarhos, G. J. U.S. Patent 5114702, 1992.
(9) WinPLOTR software at: http://www-llb.cea.fr/fullweb/winplotr/winplotr.htm.
(10) Rousse, G.; Masquelier, C.; Rodriguez-Carvajal, J.; Hervieu, M. *Electrochem. Solid-State Lett.* **1999**, *2*, 6.
(11) Katz, M. J.; Clarke, R. C.; Nye, W. F. *Anal. Chem.* **1956**, *28*, 507.
(12) Caballero, A.; Hernan, L.; Morales, J.; Sanchez, L.; Santos, J. *J. Solid State Chem.* **2003**, *174*, 365.

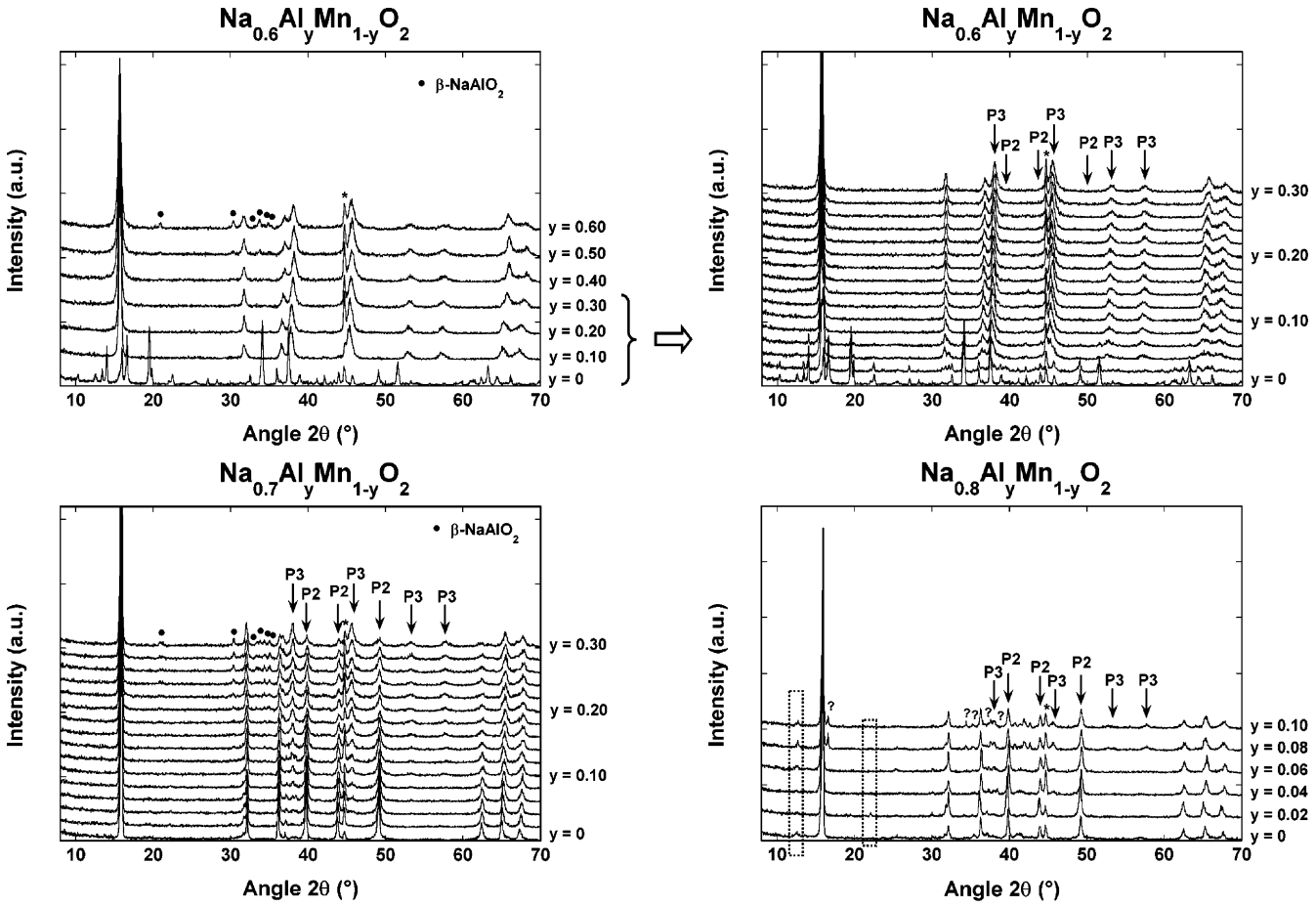

Figure 2. XRD patterns of $Na_{0.6}Al_yMn_{1-y}O_2$ ($0 \le y \le 0.30$ and $0 \le y \le 0.60$), $Na_{0.7}Al_yMn_{1-y}O_2$ ($0 \le y \le 0.30$), and $Na_{0.8}Al_yMn_{1-y}O_2$ ($0 \le y \le 0.10$) compounds or mixtures. The asterisks indicate the (200) Al peak from the sample holder, the ● symbol indicates a β-$NaAlO_2$ impurity, and question marks indicate unidentified impurities. The dashed boxes on the $Na_{0.8}Al_yMn_{1-y}O_2$ patterns highlight reflections from hydrated phases.

Table 1. Nominal and Actual Compositions of Selected Al-Substituted Phases

	compositions determined by ICP[a]	
nominal composition	before ion-exchange	after ion-exchange
$Na_{0.7}MnO_2$	$Na_{0.632}MnO_{2+z}$	$Li_{0.484}Na_{0.067}MnO_{2+z}$
$Na_{0.7}Al_{0.16}Mn_{0.84}O_2$	$Na_{0.610}Al_{0.155}Mn_{0.845}O_{2+z}$	$Li_{0.543}Na_{0.032}Al_{0.156}Mn_{0.844}O_{2+z}$
$Na_{0.6}Al_{0.16}Mn_{0.84}O_2$	$Na_{0.574}Al_{0.166}Mn_{0.834}O_{2+z}$	$Li_{0.431}Na_{0.024}Al_{0.154}Mn_{0.846}O_{2+z}$

[a] Determination of z is discussed in the text.

solutions. The limits are extended when the sodium content is decreased. Phase-pure materials form when $y \le 0.2$ for $Na_{0.7}Al_yMn_{1-y}O_2$ and $y \le 0.4$ for $Na_{0.6}Al_yMn_{1-y}O_2$ compounds. Above these levels, mixtures containing β-$NaAlO_2$ are obtained, and for $y \le 0.06$ in the $Na_{0.6}Al_yMn_{1-y}O_2$ system, the mixtures contain tunnel compounds related to $Na_{0.44}MnO_2$.[13]

Determination of the lattice parameters of the pure phases (Table 2), show some general trends. As expected, for constant x, $\mathbf{a}_{P2}$ and $\mathbf{a}_{P3}$ decrease slightly when y is increased. The lattice parameter **a** is sensitive to changes in the average (Mn, Al)−O bond length, as it lies in the basal plane of the layered structure. Substitution causes an increase in the relative amount of Mn^{4+} ions, and Al^{3+} and Mn^{4+} ($r_{Al3+} \approx r_{Mn4+} \approx 0.53$ Å)[14] are smaller than high spin Mn^{3+} ($r_{Mn3+} \approx 0.64$ Å), causing **a** to become smaller. There is a roughly inverse linear correlation of cell volume vs Al content for both P2 and P3 components (Vegard's plots), indicating that solid solutions are formed for the ranges of compositions included in Table 2. Finally, both **c** parameters become larger when x decreases due to the increase of the electrostatic repulsions between the oxygen atoms of consecutive (Mn, Al) layers.

Figure 3 shows the phase diagram of the quaternary Na−Mn−Al−O system determined from the preparation of more than 40 compounds or mixtures of general formula $Na_xAl_yMn_{1-y}O_2$, using the nominal compositions. The formation of P2 and P3 compounds or P2/P3 intergrowths is very sensitive to both Na and Al content. Outside the boundaries shown in the figure, phase mixtures containing impurities are obtained (e.g., $NaAlO_2$ at high aluminum contents and tunnel type compounds at low sodium contents). The P2 domain is rather narrow, meaning that only unsubstituted (or very slightly substituted) compounds of formula $Na_xAl_yMn_{1-y}O_2$ with $x \approx 0.7-0.8$ and low y can adopt this

(13) Doeff, M. M.; Richardson, T. J.; Kepley, L. *J. Electrochem. Soc.* **1996**, *143*, 2507.
(14) Shannon, R. D. *Acta Crystallogr.* **1976**, *A32*, 751.

Table 2. Unit Cell Parameters of P2 (Space Group *P*6$_3$/*mmc*) and P3 (Space Group *R*3*m*) Components of $Na_xAl_yMn_{1-y}O_2$ Compounds

nominal composition	P2/P3 ratio	$\mathbf{a}_{P2}$ (Å)	$\mathbf{c}_{P2}$ (Å)	$\mathbf{a}_{P3}$ (Å)	$\mathbf{c}_{P3}$ (Å)
$Na_{0.8}MnO_2$[a]	100/0	2.856(1)	11.139(6)		
$Na_{0.8}Al_{0.02}Mn_{0.98}O_2$	91/9	2.865(1)	11.115(3)	2.862(1)	16.733(12)
$Na_{0.8}Al_{0.04}Mn_{0.96}O_2$	80/20	2.850(1)	11.121(3)	2.850(1)	16.755(9)
$Na_{0.8}Al_{0.06}Mn_{0.94}O_2$	85/15	2.847(1)	11.126(3)	2.847(3)	16.867(60)
$Na_{0.75}Al_{0.15}Mn_{0.75}O_2$[a]	66/34	2.846(2)	11.157(12)	2.846(2)	16.717
$Na_{0.7}MnO_2$	100/0	2.870(1)	11.146(5)		
$Na_{0.7}Al_{0.02}Mn_{0.98}O_2$	95/5	2.863(1)	11.133(4)	N/A	N/A
$Na_{0.7}Al_{0.04}Mn_{0.96}O_2$	93/7	2.860(1)	11.135(3)	2.841(6)	16.861(30)
$Na_{0.7}Al_{0.06}Mn_{0.94}O_2$	87/13	2.859(1)	11.138(3)	2.857(1)	16.833(27)
$Na_{0.7}Al_{0.08}Mn_{0.92}O_2$	83/17	2.857(1)	11.143(5)	2.856(1)	16.797(21)
$Na_{0.7}Al_{0.10}Mn_{0.90}O_2$	79/21	2.859(1)	11.137(5)	2.853(1)	16.800(18)
$Na_{0.7}Al_{0.12}Mn_{0.88}O_2$	79/21	2.858(1)	11.125(3)	2.853(1)	16.770(21)
$Na_{0.7}Al_{0.14}Mn_{0.86}O_2$	71/29	2.855(1)	11.160(5)	2.852(3)	16.766(27)
$Na_{0.7}Al_{0.16}Mn_{0.84}O_2$	66/34	2.853(1)	11.141(5)	2.851(2)	16.770(18)
$Na_{0.7}Al_{0.18}Mn_{0.82}O_2$	55/45	2.852(1)	11.158(3)	2.851(1)	16.781(15)
$Na_{0.7}Al_{0.20}Mn_{0.80}O_2$	60/40	2.851(1)	11.138(4)	2.851(2)	16.777(18)
$Na_{0.6}Al_{0.08}Mn_{0.92}O_2$	23/77	2.839(1)	11.231(5)	2.863(1)	16.885(9)
$Na_{0.6}Al_{0.10}Mn_{0.90}O_2$	0/100			2.861(1)	16.915(11)
$Na_{0.6}Al_{0.12}Mn_{0.88}O_2$	0/100			2.861(1)	16.915(9)
$Na_{0.6}Al_{0.14}Mn_{0.86}O_2$	0/100			2.848(1)	16.881(9)
$Na_{0.6}Al_{0.16}Mn_{0.84}O_2$	0/100			2.852(1)	16.848(11)
$Na_{0.6}Al_{0.18}Mn_{0.82}O_2$	0/100			2.853(1)	16.900(9)
$Na_{0.6}Al_{0.20}Mn_{0.80}O_2$	0/100			2.852(1)	16.890(9)
$Na_{0.6}Al_{0.22}Mn_{0.78}O_2$	0/100			2.849(1)	16.875(9)
$Na_{0.6}Al_{0.24}Mn_{0.76}O_2$	0/100			2.846(1)	16.874(9)
$Na_{0.6}Al_{0.26}Mn_{0.74}O_2$	0/100			2.844(1)	16.873(9)
$Na_{0.6}Al_{0.28}Mn_{0.72}O_2$	0/100			2.842(1)	16.880(11)
$Na_{0.6}Al_{0.30}Mn_{0.70}O_2$	0/100			2.840(1)	16.847(8)
$Na_{0.6}Al_{0.40}Mn_{0.60}O_2$	0/100			2.830(1)	16.893(9)

[a] These compounds contained minor impurities.

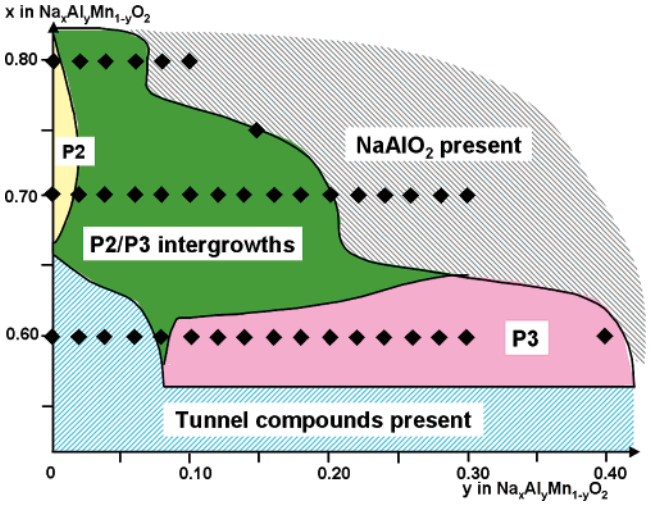

Figure 3. Approximate nominal composition range of layered P2, P3, and P2/P3 intergrowths in the Na−Al−Mn−O system.

structural form. In contrast, P3 compounds can be prepared for $0.10 \leq y \leq \sim 0.4$ in $Na_xAl_yMn_{1-y}O_2$ with $x \approx 0.6$. P2/P3 intergrowths (Table 2) exist at intermediate compositions with the relative amounts of these two stacking arrangements varying with x and y. It is interesting to note that no P2 sodium aluminum oxide analogue to the manganese-containing compound exists, to the best of our knowledge. This, or the strong tendency to form $NaAlO_2$ phases when the sodium content is raised, may explain the greater propensity for P3 formation as y in $Na_xAl_yMn_{1-y}O_2$ is increased.

Table 1 shows the results of the elemental analyses by ICP of selected samples. Note the true compositions, particularly the exact sodium content, differ slightly from the nominal ones. Some sodium vaporizes during combustion, leading to lower values than expected in the products. Additionally, transition metal vacancies are possible, leading to nonzero values of z in $Na_xAl_yMn_{1-y}O_{2+z}$, as discussed below. Based on the results in Table 1 and Figure 3 (and adjusting by 0.05−0.10 in x to correct for the differences between nominal and actual compositions), x in $Na_xAl_yMn_{1-y}O_{2+z}$ can be estimated to be about 0.5−0.6 for P3, about 0.6−0.7 for P2 phases, and somewhere between these ranges for intergrowths.

Unsubstituted P2 phases commonly have vacancies in the transition metal layers (i.e., z in Na_xMnO_{2+z} is nonzero) and the number of cationic deficiencies varies with the synthetic conditions. However, for any given set of conditions, there is almost no range of composition for x (i.e., P2-Na_xMnO_{2+z} is a line phase). P2-Na_xMnO_{2+z} may also be written $Na_{0.70(2/2+z))}Mn_{(2/2+z))}O_2$ (the crystallographic formula),[15] indicating the diminishing transition metal and sodium content as z is raised. There is a corresponding decrease in density and increase in the **c** lattice parameters due to the decrease in sodium between the transition metal layers, as well. This allows a determination of z to be made from measuring the density of a sample and comparing its lattice parameters to those of compounds with known z.[16] For example, Hagenmuller et al. described the preparation of several P2-type phases including α-$Na_{0.70}MnO_{2.25}$ ($Na_{0.62}Mn_{0.89}O_2$) at 550 °C and β-$Na_{0.70}MnO_{2.05}$ ($Na_{0.68}Mn_{0.98}O_2$,) with an orthorhombic distortion at ~630 °C.[17] The expected densities of such cation deficient samples are 3.89 and 4.22 g/cm^3, respectively, based on the reported lattice parameters. For the sample with nominal composition $Na_{0.7}MnO_2$ (i.e., $Na_{0.632}MnO_{2+z}$ ac-

(15) Delmas, A.; Fouassier, C. *Z. Anorg. Allg. Chem.* **1976**, *420*, 184.
(16) Mendiboure, A.; Delmas, C.; Hagenmuller, H. *J. Solid State Chem.* **1985**, *57*, 323.
(17) Parant, J.-P.; Olazcuaga, R.; Devalette, M.; Fouassier, C.; Hagenmuller, P. *J. Solid State Chem.* **1971**, *3*, 1.

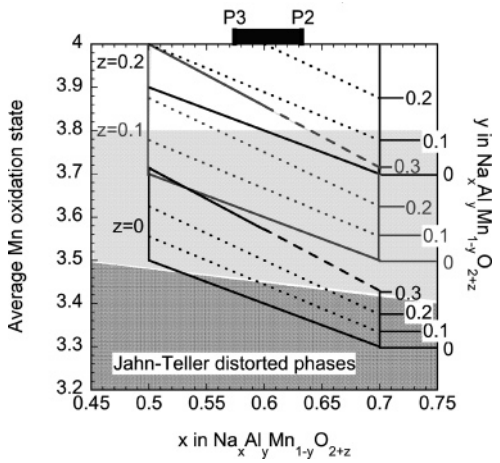

Figure 4. Average oxidation state of manganese for $Na_xAl_yMn_{1-y}O_{2+z}$ compounds as a function of *x*, *y*, and *z*.

cording to the ICP analyses), the density measurement gave 4.21 g/cm^3. Since $\rho_{calc} = 4.24$ g/cm^3 for a hypothetical phase with no vacancies, *z* can be estimated to be 0.02 for this material and the formula can be written as either $Na_{0.632}MnO_{2.02}$ or $Na_{0.614}Mn_{0.971}O_2$.

For Al-substituted phases, the crystallographic formula can be written as $Na_xAl_{y(2/2+z)}Mn_{(1-y)(2/2+z)}O_2$. There is not enough structural information available on these compounds to allow determination of *z* from density measurements, so redox titration experiments were carried out on compounds with nominal compositions P2/P3-$Na_{0.7}Al_{0.16}Mn_{0.84}O_2$ and P3-$Na_{0.6}Al_{0.16}Mn_{0.84}O_2$ instead. In theory, the average oxidation state of Mn can be measured using this method, and, in combination with the ICP results, this allows *z* to be calculated. In practice, it can be difficult to determine low values of *z* accurately. The titration experiments suggest that $z \approx 0.1$ for both the P2/P3 intergrowth and the pure P3 phases, but the error limits were too large to allow a more precise calculation.

In Figure 6 of the previous paper,[5] the effect of changing *x*, *y*, and *z* on the average oxidation state of Mn in $Na_xNi_yMn_{1-y}O_{2+z}$ was presented. Vacancies in the transition metal layer raise the average oxidation state of Mn above 3.4, reducing the cooperative Jahn−Teller effect that distorts the unit cell of the P2 phase from hexagonal to orthorhombic or monoclinic. Substitution with a +2 ion such as Ni has the same effect, and it is even possible to substitute to a level where vacancies are improbable because the average oxidation state of Mn is so high (e.g., when $y \approx 0.3$). When *x* is also reduced, as is the case when comparing idealized P3-$Na_{0.5}Ni_yMn_{1-y}O_{2+z}$ phases to P2-$Na_{0.7}Ni_yMn_{1-y}O_{2+z}$ ones, this point is reached earlier. For the former, vacancies are unlikely when $y = 0.2$, but are still possible for the latter. Thus, highly Ni-substituted P3 phases are expected to have fewer cationic deficiencies than the corresponding P2 phases or intergrowths with the same Ni content.

The effect of substitution with a +3 ion such as Al on the average Mn oxidation state is less dramatic, as Figure 4 shows. A significant portion of the $z = 0$ trapezoid encompassing $0 \le y \le 0.3$ and $0.5 \le x \le 0.7$ falls in the dark-shaded area where a cooperative Jahn−Teller effect causes an orthorhombic or monoclinic distortion of the unit cell. Because all of the phases in this study could be refined in undistorted hexagonal space groups satisfactorily, this implies that the compositions in this region of the graph must have some transition metal vacancies. No part of this trapezoid crosses into the unshaded region where the average Mn oxidation state is above about 3.8 and these types of defects are less likely. By comparing the $z = 0$ and $z = 0.1$ trapezoids, it can also be seen that increasing *z* shifts the oxidation states upward into the light-shaded region designating undistorted phases where vacancies are possible. Thus, even at high levels of substitution, cationic deficiencies in the transition metal layer are possible in P2 and P3 phases as well as in intergrowths, and highly likely in the case of low substitution levels.

Structural Characterization of $Li_xAl_yMn_{1-y}O_2$. Upon exchange of Na for Li, P2 and P3 stacking arrangements convert to O2 and O3, respectively. Li^+ ions are better accommodated in octahedral sites within the interlayers, because they are smaller than Na^+ ions. The transition metal layers simply glide to change the alkali metal environment from prismatic to octahedral coordination.[18,19] Note that conversion of P2 to O3, or P3 to O2, requires substantial rearrangement of the lattice (breaking of all the M−O bonds) and should not occur under the mild conditions used for exchange in this study. That means the O2/O3 ratios in the ion-exchanged products should be identical to the P2/P3 ratios determined in the sodium counterparts. Satisfactory Rietveld refinement of the X-ray diffraction patterns of the ion-exchanged materials was not possible because of the significant peak broadening (Figure 5), caused by a decrease in the particle size during ion exchange and an increase of stacking faults.[20] It was, however, possible to determine lattice parameters using full pattern matching refinements. For the phases in this study, $\mathbf{a}_{O2} \approx \mathbf{a}_{O3} \approx 2.8$ Å, $\mathbf{c}_{O2} \approx 9.7$ Å, and $\mathbf{c}_{O3} \approx 14.5$ Å. As expected, the Li phases have a smaller **c** parameter than the corresponding Na phases because of the smaller ionic radius of Li^+ ($r_{Li+} = 0.76$ Å) compared to Na^+ ($r_{Na+} = 1.02$ Å). For $Li_{0.8}Al_yMn_{1-y}O_2$ and $Li_{0.7}Al_yMn_{1-y}O_2$ compounds, a small impurity peak was observed at $2\theta = 15.8-15.92°$, corresponding to a layered phase containing sodium. No such peak was observed in the XRD patterns of $Li_{0.6}Al_yMn_{1-y}O_2$ compounds, which have primarily the O3 structure. This shows that ion exchange is less efficient for P2 phases than for pure P3 ones, or intergrowths with high P3 content. Nevertheless, Table 1 indicates that some sodium is still retained in O3 phases and intergrowths, either as surface contaminants or in the van der Waals gaps. If the latter, this is consistent with the presence of transition metal vacancies, which can act as traps for interlayer Na and prevent full exchange from occurring.

The redox titration of the products of the ion-exchange of P2/P3-$Na_{0.7}Al_{0.16}Mn_{0.84}O_2$ and P3-$Na_{0.6}Al_{0.16}Mn_{0.84}O_2$ indicates a decrease of the oxidation state of manganese from ~3.7 to 3.6, and *z* is estimated to be close to 0. The exchange

(18) Tournadre, F.; Croguenec, L.; Saadoune, I.; Carlier, D.; Shao-Horn, Y.; Willmann, P.; Delmas, C. *J. Solid State Chem.* **2004**, *177*, 2797.
(19) Tournadre, F.; Croguenec, L.; Willmann, P.; Delmas, C. *J. Solid State Chem.* **2004**, *177*, 2803.
(20) Wei, M.; Lu, Y.; Evans, D. G.; Duan, X. *Solid State Ionics* **2003**, *161*, 133.

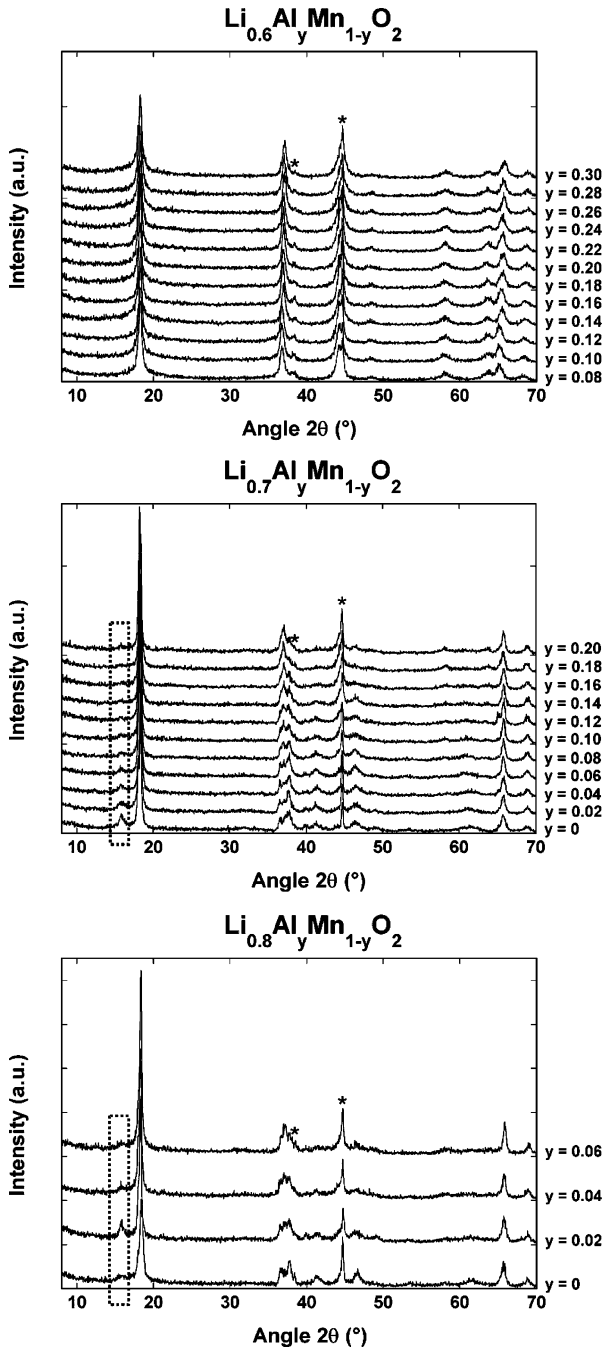

Figure 5. XRD patterns of $Li_{0.6}Al_yMn_{1-y}O_2$ ($0.08 \leq y \leq 0.30$), $Li_{0.7}Al_yMn_{1-y}O_2$ ($0 \leq y \leq 0.20$), and $Li_{0.8}Al_yMn_{1-y}O_2$ ($0 \leq y \leq 0.06$). The asterisks indicate the (111) and (200) Al peaks from the sample holder. The dashed boxes on the $Li_{0.7}Al_yMn_{1-y}O_2$ and $Li_{0.8}Al_yMn_{1-y}O_2$ patterns contain reflections from a P2-type phase containing Na ions.

conditions are slightly reducing but Table 1 indicates that the total alkali metal content has actually decreased slightly. It is possible that some oxygen from the lattice was lost concurrently with the alkali metal ions during reflux in air, although this is somewhat surprising given the mild conditions of the reaction. Unfortunately, the large error limits preclude any definitive conclusions about this or the precise value of *z*, although the sodium content found for the ion-exchanged products listed in Table 1 suggest that *z* is not exactly 0.

Electrochemical Characterization. Figure 6 shows the 1st, 10th, and 20th discharges of three distinct

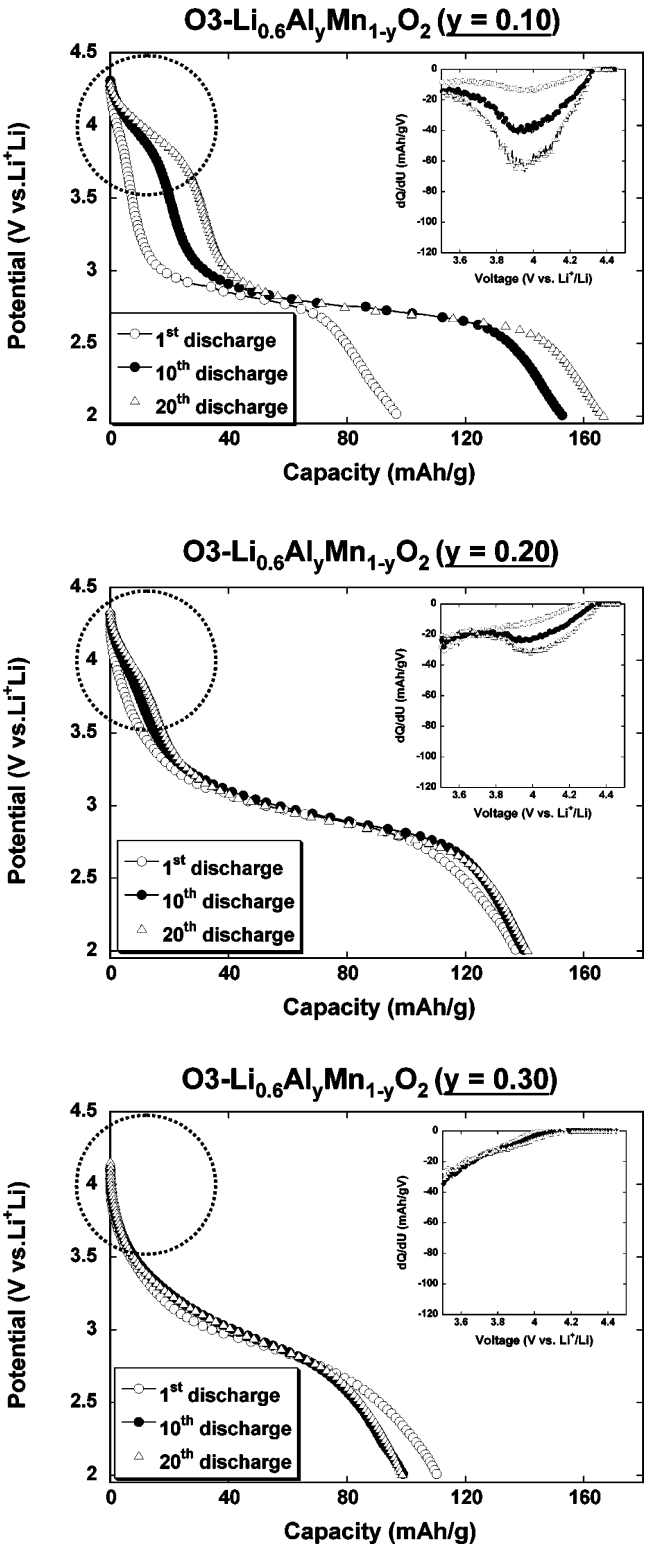

Figure 6. 1st, 10th, and 20th discharges at 0.055 mA/cm^2 of Li/1 M $LiPF_6$ EC-DMC/O3-$Li_xAl_yMn_{1-y}O_2$ ($y = 0.10$, 0.20, and 0.30) cells between 2.0 and 4.5 V. Corresponding differential capacity data are shown in the inserts.

O3−Li_xAl_y-$Mn_{1-y}O_2$ compositions ($y = 0.10$, $y = 0.20$, and $y = 0.30$). For the $y = 0.10$ sample, conversion into a spinel-like structure appears to occur as soon as the first cycle, as suggested by the development of the characteristic two-plateau voltage profile. This is fairly typical of O3 layered manganese oxides because the spinel structure is energetically favored when the composition $Li_{0.5}MO_2$ is reached. The layered to spinel conversion that occurs upon electrochemical

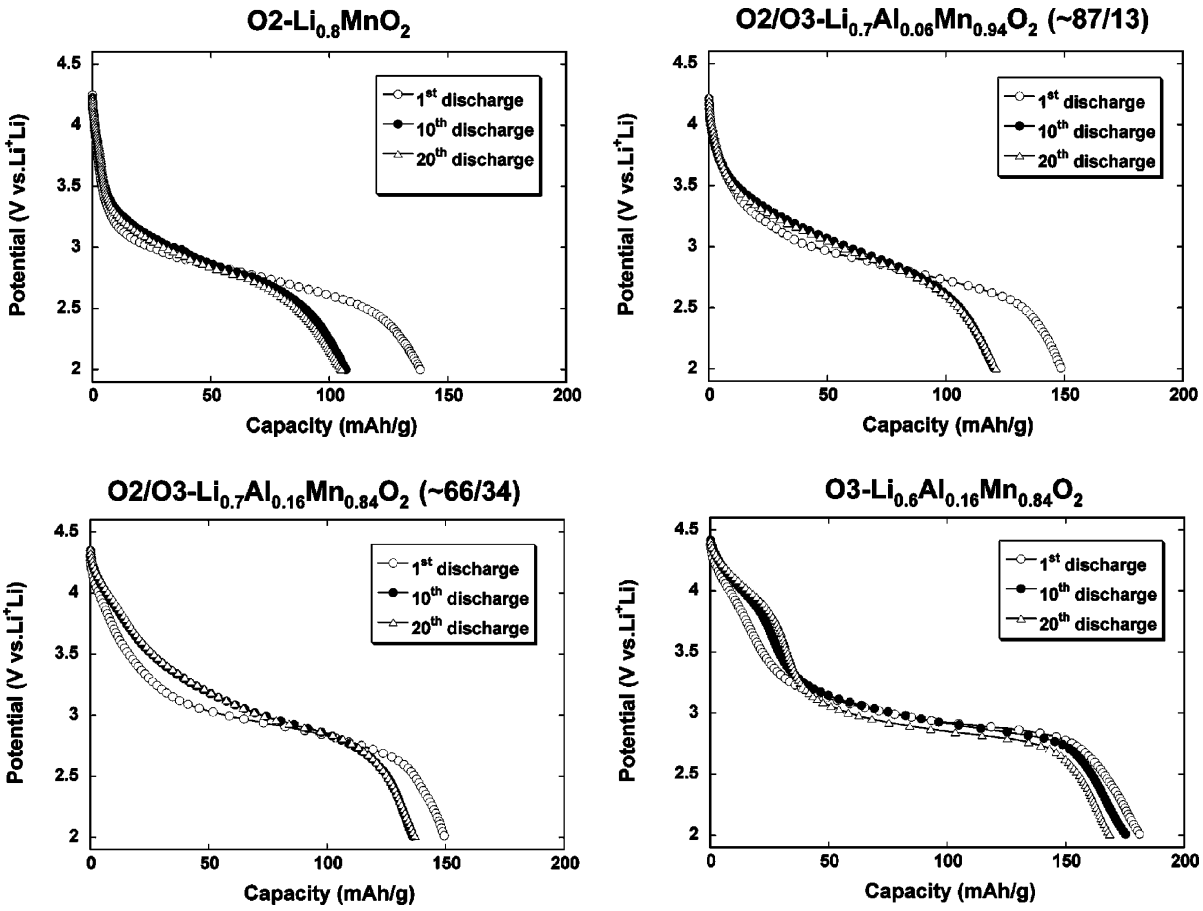

Figure 7. 1st, 10th, and 20th discharges at 0.055 mA/cm^2 of Li/1 M $LiPF_6$ EC-DMC/$Li_xAl_yMn_{1-y}O_2$ cells between 2.0 and 4.5 V. Four positive electrode materials with differing O2 and O3 contents are presented, including a pure O2 phase, two intergrowths, and a pure O3 phase.

cycling has been previously observed using TEM,[21] micro-Raman,[22] and neutron diffraction coupled with NMR[23] studies. Incremental capacity plots, which are sensitive to changes in the voltage profile, allow the formation of a spinel-like structure to be monitored, and show how the capacity in the 4-V region increases with the cycle number (insets, Figure 6). A comparison of the data for $y = 0.10$, 0.20, and 0.30 shows that the conversion slows as y becomes larger. Reed et al.[24] have suggested that partial substitution with fixed low valent cations such as Al^{3+} or multivalent cations more electronegative than Mn can suppress or prevent the phase conversion by limiting the number of Mn^{3+} ions when vacancies are present in the van der Waals gaps. This appears to be confirmed by the data in Figure 6, although complete suppression does not occur even at the 30% substitution level; after about 50 cycles for this sample, a 4-V feature begins to develop (not shown). The very high levels of substitution required to stabilize O3 electrodes completely is likely to result in unacceptably low energy densities, because Al is not redox active. It should also be noted that it may be possible for Al to migrate either to the tetrahedral sites adjacent to the transition metal layers in these structures, or to the Li sites themselves.[25] This process may eventually lead to formation of a spinel with Al partially occupying 8a and/or 16d sites (both mixed and normal Al-containing spinel structures are known). Thus, substitution with Al is unlikely to be a permanent solution for stabilizing electrodes with 100% O3 stacking arrangements.

The resistance of O2 structure types to spinel conversion during cycling has been described previously[26,27] and is further confirmed by our experiments, as is shown in Figure 7 (upper left) for O2-$Li_{0.8}MnO_2$. Unfortunately, the rate capability, practical capacity, and cycling behavior of this particular compound are disappointing. The capacity retention appears somewhat better in a slightly substituted O2/O3 intergrowth analogue (Figure 7, upper right) and there still is no development of a 4-V feature indicative of phase conversion after twenty cycles.

The two graphs at the bottom of Figure 7 compare the discharge characteristics of two 16% Al-substituted samples with differing O3 contents. Spinel conversion is fairly rapid in the case of the 100% O3 material (bottom right); by about the 10th cycle, a two-plateau profile is evident. In contrast, the 34% O3 compound (bottom left) remains stable over 20 cycles.

(21) Shao-Horn, Y.; Hackney, S. A.; Armstrong, A. R.; Bruce, P. G.; Gitzendanner, R.; Johnson, C. S.; Thackeray, M. M. *J. Electrochem. Soc.* **1999**, *146*, 2404.
(22) Hwang, S.-J.; Park, H.-S.; Choy, J.-H.; Campet, G.; Portier, J.; Kwon, C.-W.; Etourneau, J. *Electrochem. Solid-State Lett.* **2001**, *4*, 213.
(23) Armstrong, A. R.; Robertson, A. D.; Dupre, N.; Grey, C. P.; Bruce, P. G. *Chem. Mater.* **2004**, *16*, 3106.
(24) Reed, J.; Ceder, G. *Chem. Rev.* **2004**, *104*, 4513.
(25) Reed, J. Personal communication.
(26) Shaju, K. M.; Subba Rao, G. V.; Chowdari, B. V. R. *Electrochem. Commun.* **2002**, *4*, 633.
(27) Paulsen, J. M.; Thomas, C. L.; Dahn, J. R. *J. Electrochem. Soc.* **1999**, *146*, 3560.

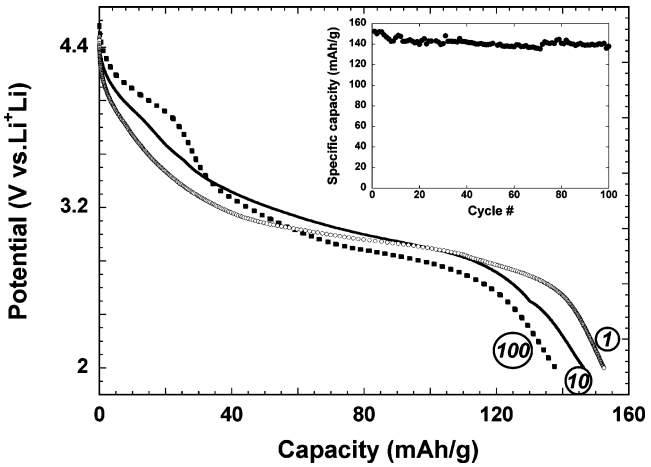

Figure 8. 1st, 10th, and 100th discharges in a lithium cell of O2O3 $Li_{0.75}Al_{0.15}Mn_{0.85}O_2$ (66/34) at 0.055 mA/cm^2 between 2.0 and 4.6 V. Discharge capacities as a function of cycle number are shown in the inset.

We have previously suggested[3] that it should be possible to design phase-conversion resistant electrodes with good electrochemical properties by exploiting the intergrowth concept. Phase conversion in O3 layers may be inhibited due to pinning by surrounding O2 layers, thus preventing the long-range ordering necessary to form spinel. Figure 8 shows an example of this concept for a cell containing the O2/O3-$Li_{0.7}Al_{0.15}Mn_{0.85}O_2$ (66/34) electrode. Only after about 100 cycles does the 4-V feature characteristic of spinel become evident. The voltage profile still has a slope, which is characteristic of layered compounds, however, rather than the two-plateau shape common to manganese oxide spinels. The capacity retention is also better than that of a pure O2 compound.

Cycling data for cells containing most of the $Li_xAl_yMn_{1-y}O_2$ cathode materials listed in Table 2 are shown in Figure 9. The top graph shows results from the pure O3 compounds with nominal compositions $Li_{0.6}Al_yMn_{1-y}O_2$ ($0.1 \le y \le 0.3$), the middle graph shows those from $Li_{0.7}Al_yMn_{1-y}O_2$ ($0 \le y \le 0.2$) O2/O3 intergrowths and the pure O2 compound $Li_{0.7}MnO_2$, and the bottom graph shows those from intergrowths with large amounts of O2 component, $Li_{0.8}Al_yMn_{1-y}O_2$ ($0 \le y \le 0.06$) and the pure O2 compound $Li_{0.8}MnO_2$. Initial capacities range from about 100 mAh/g to nearly 200 mAh/g, with values clustering rather narrowly near 150 mAh/g for most of the intergrowths and pure O2 examples. The two poorest performing compounds include heavily substituted O3-$Li_{0.6}Al_{0.3}Mn_{0.7}O_2$ and the O2/O3-$Li_{0.7}Al_{0.02}Mn_{0.98}O_2$ (95/5) intergrowth, which was exchanged a second time in hexanol to remove a residual sodium-containing phase. It is clear that this process resulted in some deterioration of the cathode material. Bruce et al. have observed superior electrochemical performance for O3-(Na, Li)$_x$Co$_y$Mn$_{1-y}$O$_2$ and O3-(Na, Li)$_x$Ni$_y$Mn$_{1-y}$O$_2$ compounds[28,29] exchanged in ethanol at 80−90 °C compared to those exchanged in hexanol at 150 °C. This is, in part, due to the beneficial effect of residual sodium ions, which slow the phase conversion of the O3 stacking arrangement, for materials exchanged under the milder conditions. It may also be possible, particularly in the case of the Al-substituted materials, for ion mixing (i.e., migration of transition metal ions to Li sites and vice versa) to occur during exchange, especially at higher temperatures, adversely impacting the electrochemical properties.

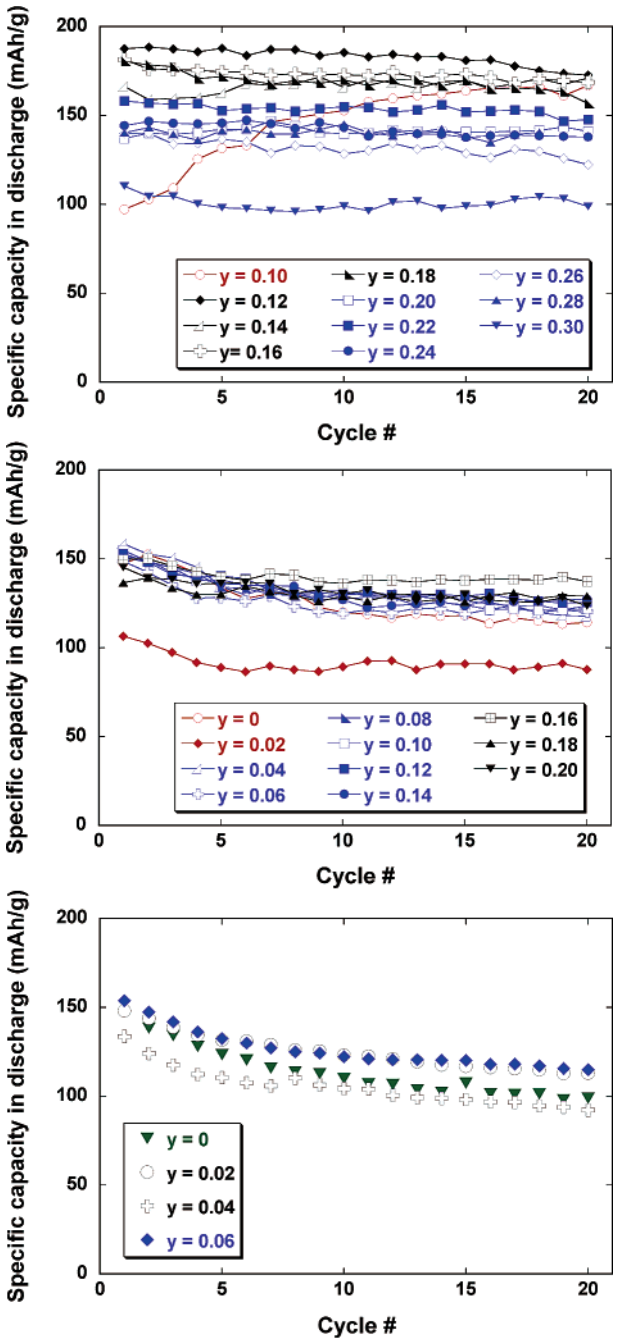

Figure 9. Discharge capacity as a function of cycle number for Li/1 M $LiPF_6$ EC-DMC/$Li_xAl_yMn_{1-y}O_2$ cells charged and discharged at 0.055 mA/cm^2 between 4.5 and 2.0 V: top, O3-$Li_{0.6}Al_yMn_{1-y}O_2$ ($0.1 \le y \le 0.30$); middle, O2/O3 $Li_{0.7}Al_yMn_{1-y}O_2$ ($0.02 \le y \le 0.2$) and O2-$Li_{0.7}MnO_2$; and bottom, O2/O3 $Li_{0.8}Al_yMn_{1-y}O_2$ ($0.02 \le y \le 0.06$) and O2-$Li_{0.8}MnO_2$.

The top graph in Figure 9 allows the effect of changing y upon the initial capacity to be observed for a series in which the stacking arrangement remains constant. Increasing y in O3-$Li_xAl_yMn_{1-y}O_2$ lowers the theoretical capacity (Table 3), because inactive Al replaces some of the electroactive Mn. Practical capacities are significantly lower than the theoretical

(28) Robertson, A. D.; Armstrong, A. R.; Fowkes, A. J.; Bruce, P. G. *J. Mater. Chem.* **2001**, *11*, 113.
(29) Quine, T. E.; Duncan, M. J.; Armstrong, A. R.; Robertson, A. D.; Bruce, P. G. *J. Mater. Chem.* **2000**, *10*, 2838.

Table 3. Electrochemical Characteristics of O3-$Li_{0.6}Al_yMn_{1-y}O_2$ Compounds

nominal composition	capacity, mAh/g theoretical[a]	capacity, mAh/g actual[b]	% of theoretical obtained on first cycle
$Li_{0.6}Al_{0.1}Mn_{0.9}O_2$	264	96	36
$Li_{0.6}Al_{0.12}Mn_{0.88}O_2$	260	188	72
$Li_{0.6}Al_{0.14}Mn_{0.86}O_2$	256	167	65
$Li_{0.6}Al_{0.16}Mn_{0.84}O_2$	251	181	71
$Li_{0.6}Al_{0.18}Mn_{0.82}O_2$	247	193	77
$Li_{0.6}Al_{0.20}Mn_{0.80}O_2$	243	136	56
$Li_{0.6}Al_{0.22}Mn_{0.78}O_2$	238	160	67
$Li_{0.6}Al_{0.24}Mn_{0.76}O_2$	233	144	62
$Li_{0.6}Al_{0.26}Mn_{0.74}O_2$	229	140	61
$Li_{0.6}Al_{0.28}Mn_{0.72}O_2$	224	140	62
$Li_{0.6}Al_{0.30}Mn_{0.70}O_2$	219	110	50

[a] Based on a nominal discharged composition of $LiAl_yMn_{1-y}O_2$ and assuming z is 0. [b] Obtained on first full discharge.

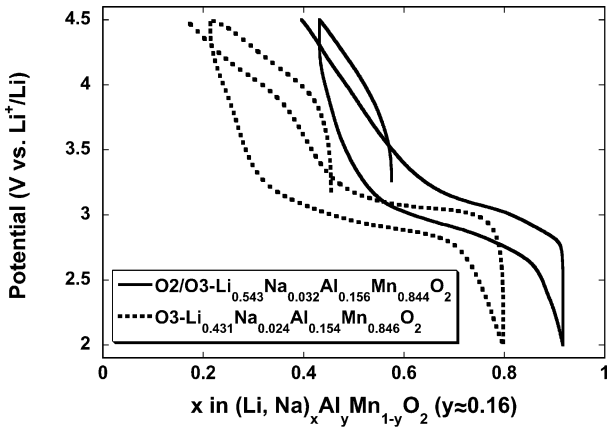

Figure 10. Initial charges and subsequent first cycles of lithium cells containing O3-$Li_{0.6}Al_{0.16}Mn_{0.84}O_2$ and O2/O3-$Li_{0.7}Al_{0.16}Mn_{0.84}O_2$ (nominal compositions) at 0.055 mA/cm^2 between 2.0 and 4.5 V. The true compositions as determined by ICP are given in the figure key.

ones in many cases, however, and no adverse effect of increasing Al substitution upon capacity is seen below about 18%. Nearly all the compounds could be deintercalated almost to the expected limit (assuming that the alkali metal content is slightly less than the nominal values), suggesting that z is low for most members of the series. Electrodes that delivered significantly less than the theoretical capacity appeared to do so because they could not be discharged fully. If some Al is located in Li sites, or migrates there during cycling, it can block diffusion and result in lower than expected discharge capacities.

The effect of changing the stacking arrangement can be determined by comparing results in the bottom two graphs of Figure 9 for O2 structures and O2/O3 intergrowths to those in the top graph for the pure O3 compounds. In the case of 20% Ni substitution,[5] there was a dramatic decrease in the discharge capacity as the proportion of O2 component rose. The effect is more ambiguous, however, for the Al-substituted compounds. For the 16% Al-substituted examples shown at the bottom of Figure 7, the initial capacity drops somewhat from about 180 mAh/g for a pure O3 compound to 150 mAh/g for one that is 34% O3. This difference is mainly attributable to the inability to extract as much lithium during the first charge for the latter compared to the former (Figure 10).

While it was generally true that electrodes containing more O3 component could be charged further initially, this did not always translate into higher capacities upon the subsequent discharge. Some electrodes with the same level of Al-substitution but higher O2 content actually were slightly better than those with more O3 component. (Compare, for example, O2/O3-$Li_{0.8}Al_{0.04}Mn_{0.96}O_2$ (80/20) in the bottom graph with O2/O3-$Li_{0.7}Al_{0.04}Mn_{0.96}O_2$ (93/7) in the middle graph). O3 content generally increases as the Al-substitution levels are raised for both the $Li_{0.8}Al_yMn_{1-y}O_2$ and $Li_{0.7}Al_yMn_{1-y}O_2$ series shown in Figure 10, but the effect of this on the initial practical capacities is minimal. As with the pure O3 compounds, best results are obtained for a substitution level of about 12−18% Al, but the full theoretical capacities are not achieved with any of these compounds.

Varying numbers of transition metal vacancies, the electrochemical inactivity of Al and the trend toward higher O3 content as y in $Li_xAl_yMn_{1-y}O_2$ is increased, and the possibility of Al migration into the van der Waals gaps (which can also occur in O2 structures but will not lead to spinel formation) affect the electrochemical capacities in complex ways. Therefore, there is not as strong a correlation between the observed practical capacity and the O3 content as there is in the Ni-substituted system, which has fewer of these competing trends.

The most beneficial effect of increased O3 content for the Al-substituted compounds appears to be an improvement in the capacity retention upon cycling rather than an overall improvement in energy density. Figure 9 shows that capacity fading upon cycling of O3 compounds is low, despite the rapid phase conversion of many of these electrodes. The improved cycling behavior of electrochemically transformed spinels compared to traditionally synthesized ones has been noted in several previous studies.[30,31] This has been attributed to the formation of nanodomains[32] that can provide ferroelastic accommodation of transformation strains.[33−35] Fading upon cycling is more evident in the electrodes with high O2 content shown in Figure 9. The intergrowths (middle graph) show intermediate behavior with better capacity retention than pure O2 compounds and better phase stability than O3 ones.

Intercalation processes for some pure O2 layered manganese oxide compounds appear to be more kinetically limited than for O3 structures.[3] This results in a falloff of capacity for cells containing O2 electrodes when the current density is increased even modestly. Another possible advantage toward using intergrowth electrodes rather than pure O2 ones, therefore, is improved rate capability. Figure 11 shows the results of rate studies on cells containing O2/O3-$Li_{0.7}Al_{0.16}Mn_{0.84}O_2$ and O3-$Li_{0.6}Al_{0.16}Mn_{0.84}O_2$ compounds. The top graphs show cycling data at three different

(30) Armstrong, A. R.; Paterson, A. J.; Robertson, A. D.; Bruce, P. G. *Chem. Mater.* **2002**, *14*, 710.
(31) Gummow, R. J.; Liles, D. C.; Thackeray, M. M. *Mater. Res. Bull.* **1993**, *28*, 1249.
(32) Poizot, P.; Laruelle, S.; Grugeon, S.; Dupont, L.; Tarascon, J.-M. *Nature* **2000**, *407*, 496.
(33) Robertson, A. D.; Armstrong, A. R.; Bruce, P. G. *Chem. Mater.* **2001**, *13*, 2380.
(34) Shao-Horn, Y.; Hackney, S. A.; Armstrong, A. R.; Bruce, P. G.; Gitzendanner, R.; Johnson, C. S.; Thackeray, M. M. *J. Electrochem. Soc.* **1999**, *146*, 2404.
(35) Jang, Y. I.; Huang, B.; Wang, H.; Sadoway, D. R.; Chiang, Y. M. *J. Electrochem. Soc.* **1999**, *146*, 3217.

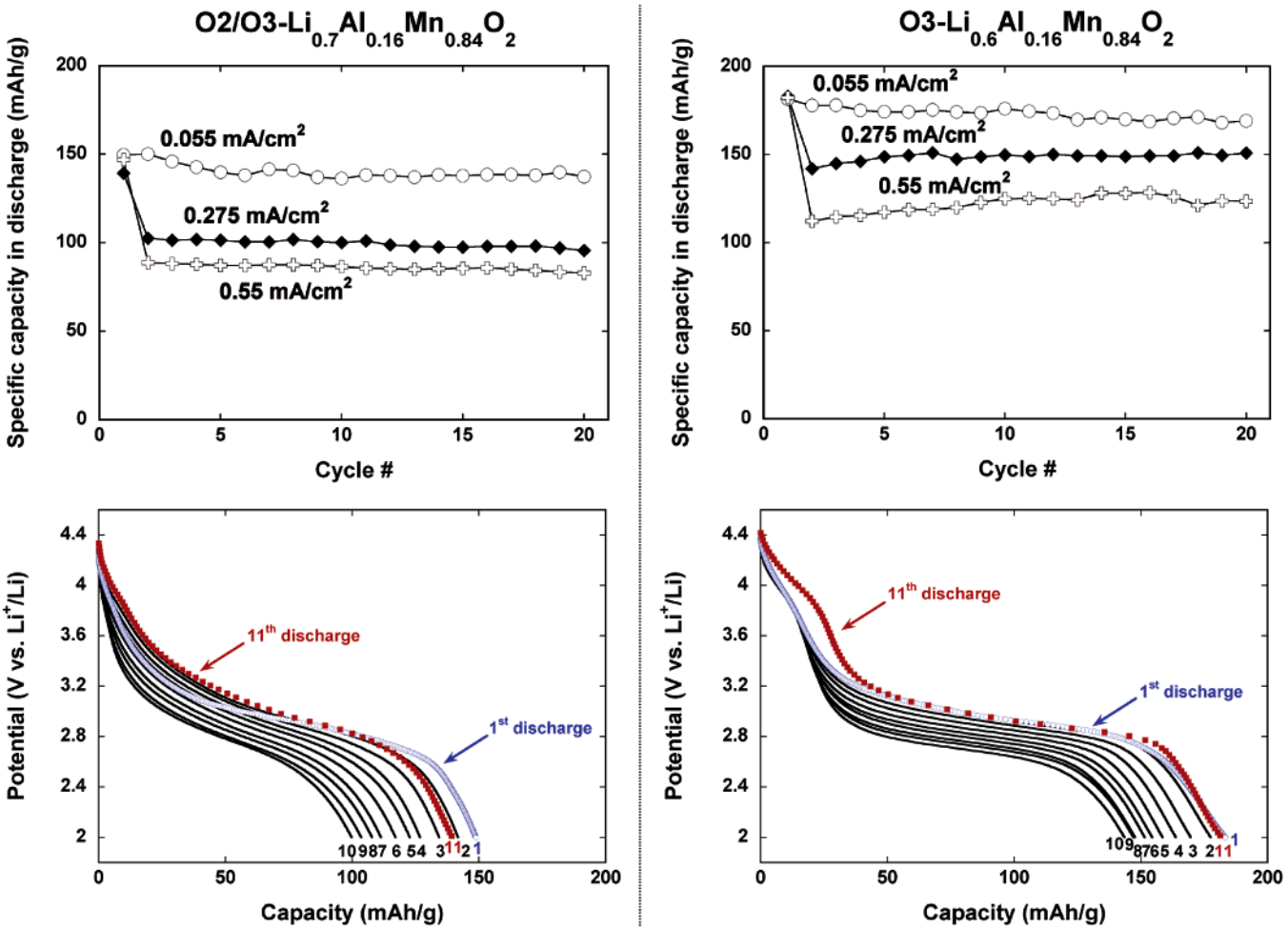

Figure 11. Top: Discharge capacity as a function of cycle number and current density for Li/1 M $LiPF_6$ EC-DMC/O2/O3-$Li_{0.7}Al_{0.16}Mn_{0.84}O_2$ and Li/1 M $LiPF_6$ EC-DMC/O3-$Li_{0.6}Al_{0.16}Mn_{0.84}O_2$ cells cycled between 2.0 and 4.5 V. Bottom: Successive discharges of Li/1 M $LiPF_6$ EC-DMC/O2/O3-$Li_{0.7}Al_{0.16}Mn_{0.84}O_2$ and Li/1 M $LiPF_6$ EC-DMC/O3-$Li_{0.6}Al_{0.16}Mn_{0.84}O_2$ cells between 4.5 and 2.0 V at various current densities (1st and 11th discharges at 0.055 mA/cm^2, 2nd at 0.11 mA/cm^2, 3rd at 0.165 mA/cm^2, 4th at 0.22 mA/cm^2, 5th at 0.275 mA/cm^2, 6th at 0.33 mA/cm^2, 7th at 0.385 mA/cm^2, 8th at 0.44 mA/cm^2, 9th at 0.495 mA/cm^2, and 10th at 0.55 mA/cm^2.

current densities and the lower graphs show a series of discharge profiles at varying rates. Cycling at higher current densities does not result in a greater rate of fade for either type of electrode, indicating that both systems are fairly robust. For both electrodes, there is a moderate decrease in the delivered capacity when the current density is increased 10-fold (bottom graphs of Figure 11), by about 21% and 33% for the pure O3 and O2/O3 intergrowth, respectively. The higher percentage for the intergrowth implies a somewhat worse rate capability, but this is partly due to the different area capacities of the two electrodes. A fairer comparison is shown in Figure 12, where the data has been normalized to account for the differing electrode thicknesses by converting current densities into C-rates. A 1 C rate means full discharge in 1 h, based on the capacity obtained at low current densities, while C/10 would mean a 10-h discharge. For the cells shown in the bottom of Figure 11, 0.55 mA/cm^2 corresponds to C/2.2 for the O2/O3 electrode and C/3.8 for the O3 electrode. When presented this way, it appears that the rate capabilities of these two materials are almost exactly the same. These results indicate that it is indeed possible to design stable layered manganese oxide electrodes with good electrochemical properties by exploiting the intergrowth concept.

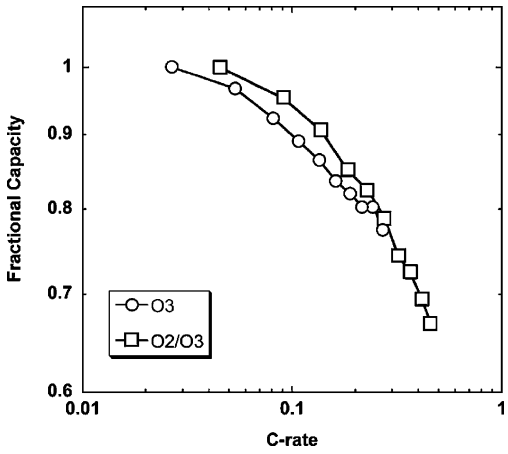

Figure 12. Rate capabilities for the two cells shown at the bottom left and bottom right of Figure 11, given in terms of C-rates and fractions of total capacities delivered at the lowest current densities.

IV. Conclusions

Layered Al-substituted manganese oxides with nominal compositions of $Na_xAl_yMn_{1-y}O_2$ were made by a combustion process. Depending upon the Na and Al content, pure P2, P3, or intergrowth structures were obtained. The lithiated analogues, prepared by an ion-exchange process, have O2,

O3, or intergrowth stacking arrangements. O3 compounds readily convert into a spinel-like structure upon cycling, although increased Al substitution delays, but does not completely prevent, this transformation. In contrast, spinel conversion is more effectively suppressed in O2/O3 intergrowth structures. Practical capacities were frequently lower than the values predicted from theory, and ranged from 100 to 200 mAh/g upon the first discharge for pure O3 structures, and about 150 mAh/g for most of the intergrowths and pure O2 compounds. Best results were obtained when the Al content was about 12−18% for pure O3 structures and the intergrowths. Interestingly, there was little effect of increasing Al content upon the practical capacity until substitution levels became very high. Unlike with $Li_xNi_{0.2}Mn_{0.8}O_2$ electrodes, capacities do not necessarily increase as O3 content is raised in every case. In the $Li_xAl_yMn_{1-y}O_2$ system, the practical capacity is affected in complex ways by several competing factors that do not exist for the $Li_xNi_yMn_{1-y}O_2$ analogues. Although increasing the O3 content in intergrowths does not necessarily result in higher cathode energy densities, it does improve the cycling behavior and rate capability of cells containing these electrodes, compared to those containing pure O2 ones. Intergrowth electrodes, therefore, have demonstrable advantages over both pure O2 electrodes and pure O3 ones.

Acknowledgment. This work was supported by the Assistant Secretary for Energy Efficiency and Renewable Energy, Office of FreedomCAR and Vehicle Technologies of the U.S. Department of Energy under Contract DE-AC03-76SF00098.

CM0484394